TMPRSS2:ERG gene fusion expression regulates bone markers and enhances the osteoblastic phenotype of prostate cancer bone metastases

Carine Delliaux, Tian Tian, Mathilde Bouchet, Anais Fradet, Nathalie Vanpouille, Anne Flourens, Rachel Deplus, Arnauld Villers, Xavier Leroy, Philippe Clézardin, et al.

Accepted Manuscript

TMPRSS2:ERG gene fusion expression regulates bone markers and enhances the osteoblastic phenotype of prostate cancer bone metastases

Carine Delliaux, Tian V. Tian, Mathilde Bouchet, Anais Fradet, Nathalie Vanpouille, Anne Flourens, Rachel Deplus, Arnauld Villers, Xavier Leroy, Philippe Clezardin, Yvan de Launoit, Edith Bonnelye, Martine Duterque-Coquillaud

PII: S0304-3835(18)30551-2

DOI: 10.1016/j.canlet.2018.08.027

Reference: CAN 14041

To appear in: *Cancer Letters*

Received Date: 26 March 2018

Revised Date: 31 July 2018

Accepted Date: 26 August 2018

Please cite this article as: C. Delliaux, T.V. Tian, M. Bouchet, A. Fradet, N. Vanpouille, A. Flourens, R. Deplus, A. Villers, X. Leroy, P. Clezardin, Y. de Launoit, E. Bonnelye, M. Duterque-Coquillaud, *TMPRSS2:ERG* gene fusion expression regulates bone markers and enhances the osteoblastic phenotype of prostate cancer bone metastases, *Cancer Letters* (2018), doi: 10.1016/j.canlet.2018.08.027.

Abstract

Prostate cancers have a strong propensity to metastasize to bone and promote osteoblastic lesions. *TMPRSS2:ERG* is the most frequent gene rearrangement identified in prostate cancer, but whether it is involved in prostate cancer bone metastases is largely unknown. We exploited an intratibial metastasis model to address this issue and we found that ectopic expression of the *TMPRSS2:ERG* fusion enhances the ability of prostate cancer cell lines to induce osteoblastic lesions by stimulating bone formation and inhibiting the osteolytic response. In line with these *in vivo* results, we demonstrate that the TMPRSS2:ERG fusion protein increases the expression of osteoblastic markers, including Collagen Type I Alpha 1 Chain and Alkaline Phosphatase, as well as Endothelin-1, a protein with a documented role in osteoblastic bone lesion formation. Moreover, we determined that the TMPRSS2:ERG fusion protein is bound to the regulatory regions of these genes in prostate cancer cell lines, and we report that the expression levels of these osteoblastic markers are correlated with the expression of the TMPRSS2:ERG fusion in patient metastasis samples. Taken together, our results reveal that the *TMPRSS2:ERG* gene fusion is involved in osteoblastic lesion formation induced by prostate cancer cells.

TMPRSS2:ERG gene fusion expression regulates bone markers and enhances the osteoblastic phenotype of prostate cancer bone metastases

Carine Delliaux [a,b,1], Tian V. Tian [a,c,1], Mathilde Bouchet [d, e], Anais Fradet [d, e], Nathalie Vanpouille [a], Anne Flourens [a], Rachel Deplus [a], Arnauld Villers [f], Xavier Leroy [g], Philippe Clezardin [d, e], Yvan de Launoit [a], Edith Bonnelye [d, e], Martine Duterque-Coquillaud [a,*]

[a]Univ. Lille, CNRS, Institut Pasteur de Lille, UMR 8161 - Mechanisms of Tumorigenesis and Target Therapies, F-59021 Lille, France

[b]Montreal Clinical Research Institute (IRCM), QC H2W 1R7, Montreal, Canada

[c]Center for Genomic Regulation (CRG), The Barcelona Institut of Science and Technology, Universitat Pompeu Fabra (UPF), Dr. Aiguader 88, S-08003 Barcelona, Spain

[d]Unité INSERM U1033, F-69372 Lyon, France

[e]Université Claude Bernard Lyon 1, F-69008 Lyon, France

[f]Département d'Urologie, CHRU, Université de Lille, F-59037 Lille , France

[g]Institut de Pathologie-Centre de Biologie-Pathologie-Centre Hospitalier Régional et Universitaire, F-59037 Lille, France

Keywords: Fusion Gene, TMPRSS2:ERG, Prostate Cancer, Bone Metastasis, Osteoblastic lesions, Transcriptional Regulation.

***Corresponding author**. Institut de Biologie de Lille, CNRS UMR8161, 1 rue du Professeur Calmette, SC50447, Lille, 59021, France.

Email address: martine.duterque@ibl.cnrs.fr

[1]These authors contributed equally to this work

Abstract

Prostate cancers have a strong propensity to metastasize to bone and promote osteoblastic lesions. *TMPRSS2:ERG* is the most frequent gene rearrangement identified in prostate cancer, but whether it is involved in prostate cancer bone metastases is largely unknown. We exploited an intratibial metastasis model to address this issue and we found that ectopic expression of the *TMPRSS2:ERG* fusion enhances the ability of prostate cancer cell lines to induce osteoblastic lesions by stimulating bone formation and inhibiting the osteolytic response. In line with these *in vivo* results, we demonstrate that the TMPRSS2:ERG fusion protein increases the expression of osteoblastic markers, including Collagen Type I Alpha 1 Chain and Alkaline Phosphatase, as well as Endothelin-1, a protein with a documented role in osteoblastic bone lesion formation. Moreover, we determined that the TMPRSS2:ERG fusion protein is bound to the regulatory regions of these genes in prostate cancer cell lines, and we report that the expression levels of these osteoblastic markers are correlated with the expression of the TMPRSS2:ERG fusion in patient metastasis samples. Taken together, our results reveal that the *TMPRSS2:ERG* gene fusion is involved in osteoblastic lesion formation induced by prostate cancer cells.

Highlights

- *TMPRSS2:ERG* gene expression enhances the osteoblastic phenotype of bone lesions
- TMPRSS2:ERG fusion-expressing tumor cells overexpress osteoblastic markers
- Expression of *Collagen Type I Alpha 1 Chain, Alkaline Phosphatase* and *Endothelin-1* is enhanced by the TMPRSS2:ERG expression
- *Collagen Type I Alpha 1 Chain*, *Alkaline Phosphatase* and *Endothelin-1* are direct target genes of ERG transcription factor

1. Introduction

Bone metastases occur in more than 80% of men who die from prostate cancer (PCa) [1]. Bone is a dynamic tissue under constant remodeling by the interplay between bone-resorbing osteoclasts and bone-forming osteoblasts. Through a process called osteomimicry, metastatic PCa cells acquire a bone cell-like phenotype that helps them to survive and proliferate within the bone microenvironment [2-4]. At the same time, tumor cells homing into bone marrow promote alterations in osteoblast and osteoclast functions [5-7]. Such reciprocal stimulations between tumor and bone cells generate a vicious circle that results in an alteration of bone structure [2]. Despite the frequent occurrence of virtually incurable bone lesion formations found in PCa, little is known about the molecular mechanisms underlying bone metastases in this disease [8].

Chromosomal rearrangements involving genes encoding ETS (E-twenty-six) transcription factors are found in more than 50% of human PCa cases and constitute the most frequent gene rearrangements in human malignancies [9, 10]. The most common ETS gene rearrangement is *TMPRSS2:ERG* which fuses the androgen-responsive promoter of *TMPRSS2* (*Transmembrane Protease, Serine 2*) to *ERG* (*ETS-related gene*), promoting its aberrant expression. This results in a significant upregulation of the ERG transcription factor [9].
Several clinical studies suggest that *TMPRSS2:ERG* fusions are associated both with poorly differentiated samples (Gleason score >6) [11-13] and with disease recurrence after surgery [14]. In contrast, additional studies suggest that these fusions can also be associated with a favorable prognosis, depending on the exact exons involved in the genomic rearrangement and on the copy number [15, 16]. Nevertheless, whatever it is, a higher dosage of ERG clearly leads to a more severe disease phenotype [15, 16]. Indeed, using PCa cell lines and diverse mouse models, several studies have demonstrated that the overexpression of TMPRSS2:ERG fusion proteins not only facilitates PCa initiation [17, 18], but also promotes both PCa cell migration and invasion [19, 20]. Mechanistically, ERG controls a transcriptional network

related to the development of PCa and its progression into a metastatic disease [21, 22]. Until now, whether and how TMPRSS2:ERG fusions are involved in the formation of PCa bone metastases remains largely unknown. Recently, our group reported that the ectopic expression of the *TMPRSS2:ERG* fusion results in an increased number of bone lesions upon intracardiac injection of PCa cells in mice [23]. This work revealed the contribution of the fusion to bone tropism associated with the metastatic progression of PCa. It is now essential to molecularly depict how TMPRSS2:ERG fusion expression acts on the interplay between the bone microenvironment and tumor cells to ultimately define novel therapeutic strategies.

Here, we aim to mechanistically dissect the role of *TMPRSS2:ERG* fusions in increasing cancer progression when the prostate tumor cells reside into the bone microenvironment. We found that after injection into the tibiae of severe combined immunodeficiency (SCID) mice, the human PCa cell lines PC3 and PC3c, which express one of the most frequent *TMPRSS2:ERG* fusions, increase the osteoblastic phenotype of bone lesions and inhibit osteoclast-mediated bone destruction. In agreement with these findings, we also demonstrated that TMPRSS2:ERG directly controls the expression of two major osteoblastic markers, *ALPL (Alkaline Phosphatase, Liver/Bone/Kidney)* and *COL1A1* (*Collagen Type I Alpha 1 Chain)*, as well as of *ET-1 (Endothelin-1)*, which has been previously demonstrated to favor the osteoblastic phenotype of bone metastases. Taken together, our results reveal that the TMPRSS2:ERG fusions is involved in the control of PCa cell-induced bone remodeling.

2. Material and Methods

2.1. Cell culture, treatment and chemical reagents

The VCaP cell line was obtained from the American Type Culture Collection (ATCC, Manassas, VA, USA), the PC3 and PC3c cells were from Edith Bonnelye (INSERM U1033, Université Claude Bernard, Lyon, France). The PC3 cell line was authenticated by STR

profiling prior to the experiments (IdentiCell, Aarhus, Denmark) and presented a 100% match with PC3. The PC3c were isolated *in vitro* from this PC3 cell line, after single cell population culture [24]. PC3 cells were cultured in F12K nutrient mixture, whereas PC3c and VCaP cells were maintained in Dulbecco's modified Eagle's medium (DMEM, Thermo Fisher Scientific, Waltham, MA, USA). All media were supplemented with 10% fetal bovine serum (FBS, Thermo Fisher Scientific, Waltham, MA, USA) and Zell Shield agent (Minerva Biolabs, Berlin, Germany). Cells were sub-cultured every 3-4 days and tested every 3 months for potential mycoplasma contamination with MycoAlert™ mycoplasma detection kit (Lonza, Basel, Switzerland). To induce *TMPRSS2:ERG* expression, VCaP cells were treated with 10 nM DHT (5α-Androstan-17β-ol-3-one) or vehicle for 16 hours. Unless otherwise stated, all chemical reagents were from Sigma-Aldrich (St Louis, MO, USA).

2.2. Generation of TMPRSS2:ERG expressing cells

PC3c clones, stably transfected with either empty pcDNA3.1 vector or *TMPRSS2:ERG* expression vector, were obtained as described previously (namely PC3c-CT, PC3c-T1E4-L, PC3c-T1E4-M and PC3c-T1E4-H) [19]. To obtain the PC3 clones, the same *TMPRSS2:ERG* cDNA was subcloned into the retroviral vector pLPCX (Clontech Laboratories, Mountain View, CA, USA). For production of the virus, 7 x 10^6 GP2-293 cells (Clontech Laboratories, Mountain View, CA, USA) were transfected with 25 µg of empty pLPCX or pLPCX/TMPRSS2:ERG, and 6 µg of pVPack-VSV-G (Clontech Laboratories, Mountain View, CA, USA) in the presence of 64 µL of Lipofectamine 2000 (Thermo Fisher Scientific, Waltham, MA, USA). After incubating for two days with fresh medium, 4 mL of the viral particle-containing supernatants were mixed with 8 µg/mL of Polybrene. This was then incubated with 0.3 x 10^6 PC3 cells in a 6-well plate in order to generate the TMPRSS2:ERG expressing cells (namely PC3-CT and PC3-T1E4). Successfully infected

cells were selected the next day by adding Puromycin (1 µg/mL) (Thermo Fisher Scientific, Waltham, MA, USA) in the culture medium for one week.

2.3. siRNA transfection

Predesigned and pooled siRNAs were obtained from GE Dharmacon (Lafayette, CO, USA). Cells were transfected with the siRNA (50 nM) using Lipofectamine 2000 reagent according to the manufacturer's instructions. Gene-knockdown effects were evaluated 72 hours after the transfection. The siRNAs used in this study were siERG (ON-TARGETplus SMARTpool L-003886-00) and the control siRNA (ON-TARGETplus Non-targeting Pool D-001810-10).

2.4. RNA extraction and gene expression analysis

Total RNA was purified using the NucleoSpin RNA kit (Macherey-Nagel, Düren, Germany) according to the manufacturer's instructions. For retrotranscription, 1 µg of total RNA was used to generate cDNA using the High Capacity RNA-to-cDNA kit (Applied Biosystems, Foster City, CA, USA). Quantitative PCRs (qPCRs) were performed using the power SYBR-Green PCR Master kit (Applied Biosystems, Foster City, CA, USA) on a Stratagene Mx3005P qPCR System (Stratagene, La Jolla, CA, USA) according to the manufacturer's instructions. The relative expression levels of individual genes were calculated using the $-2^{\Delta\Delta CT}$ method and normalized to that of the 18S or L32 housekeeping gene. Optimal primer specificity and efficiency were validated according to the Mx3005P qPCR system user's guide. The primers used in this study can be found in Supplemental Table 1.

2.5. Chromatin immunoprecipitation (ChIP)

ChIP assays were performed as described in Tian et al., 2014 [19] using either a polyclonal rabbit anti-ERG antibody (sc-353, Santa Cruz Biotech, Dallas, TX, USA) or a

control rabbit IgG antibody (Santa Cruz Biotech, Dallas, TX, USA). The genomic DNA was purified using NucleoSpin Clean-up columns (Macherey-Nagel, Düren, Germany) according to manufacturer's instructions. Immuno-precipitated genomic DNA was analyzed by PCR or qPCR, and details of the primers used in this study can be found in Supplemental Table 1.

2.6. ELISA

Conditioned media from cell culture were used for protein detection. The levels of ET-1 secreted by PC3c cells and by PC3c-CT, PC3c-T1E4-L, PC3c-T1E4-M and PC3c-T1E4-H clones were measured using a Quantikine ELISA kit (R&D Systems, Minneapolis, MN, USA).

2.7. Analysis of publicly available datasets

To analyze *ERG*, *ET-1*, *ALPL*, *COL1A1*, *OPN*, *BSP*, *OCN*, *OPG* and *RANKL* mRNA expression levels in PCa metastasis samples, we obtained the data from Beltran *et al*. by using cBioPortal for Cancer Genomics database (http://www.cbioportal.org) [25-27]. Specifically, we selected the cohort named "Neuroendocrine Prostate Cancer (Trento/Cornell/Broad 2016)" and kept only the "CRPC Adeno" disease code, corresponding only to the adenocarcinoma cases, not the neuroendocrine ones. The oncoprint shows the mRNA z-scores of 52 cases of castration resistant prostate adenocarcinoma metastases. Gene up-regulation in a given case is provided by cBioPortal as a z-score of ≥2. A z-score of 2 was defined as an array probe-set intensity that is two standard deviations greater than the mean of the probe set intensity in the matched normal tissue. Data were accessed from the cBioPortal in October 2016.

To analyze the binding of ERG to the *ALPL*, *COL1A1* and *ET-1* loci in VCaP cells, the only cell line harboring endogenous expression of TMPRSS2:ERG, we obtained the data from Asangani *et al*. (GSM1328979), Sharma *et al*. (GSM1193656, GSM1193657, GSM1193658), and Chng *et al*. (GSM717395, GSM717396, GSM717397) by using cistrome database

(http://www.cistrome.org/db) [21, 28-30]. Data were then uploaded on UCSC Browser to analyze the binding of ERG (http://www.genome.ucsc.edu) [31]. ERG ChIP-sequencing data view scaling have been modified to use a vertical viewing range setting from 0 to 3 for *ALPL*, 0 to 1 for *COL1A1* and 0 to 0.5 for *ET-1*. Tracks from the human ENCODE project for H3K27Ac and H3K4Me1 marks, often found near regulatory elements, H3K4Me3 marks, often found near promoters, as well as DNase I hypersensitivity peak clusters have been added. Data were accessed from the Cistrome and UCSC in November 2016.

2.8. Animal studies

The mice used in this study were handled according to French national rules (Décret N° 87-848 du 19/10/1987, Paris). Experimental protocols were approved by the Institutional Animal Care and Use Committee at the University Lyon-1, France (CEEA-55 Comité d'Ethique en Expérimentation Animale DR2014-32). Animal experiments were routinely inspected by the attending veterinarian to ensure continued compliance with the proposed protocols. Animals bearing tumor xenografts were carefully monitored for established signs of distress and discomfort and were humanely euthanized. Intra-osseous tumor xenograft experiments in anaesthetized mice were carried out in six-week-old SCID male mice (Charles River Laboratories, Wilmington, MA, USA). PC3 cells are known to induce pure osteolytic lesions, while PC3c cells induce mixed lesions with both osteolytic and osteoblastic regions in the bone marrow cavity [24]. PC3 and PC3c cells (6×10^5 in 15 μL PBS) were injected into the bone marrow cavity. Mice were then sacrificed after either six weeks (PC3) or 10 weeks (PC3c). Radiographs (LifeRay HM Plus, Ferrania) of animals were taken using a Faxitron MX-20 (Faxitron X-ray Corporation). The bone lesion surface, which includes both osteolytic and osteoblastic regions, was measured using the computerized image analysis system MorphoExpert (Exploranova). The extent of the bone lesions for each animal was expressed in mm^2. Once sacrificed, the hind limbs of mice were collected for histology and

histomorphometrics analyses. Tibiae were scanned using microcomputed tomography (Skyscan1174, Skyscan Kontich, Belgium) with an 8.8 voxel size and an X-ray tube (50 kV; 80 μA) with a 0.5-μm aluminum filter. Three-dimensional reconstructions and rendering were performed using the manufacturer's software packages NRecon & CTVox, and Skyscan, respectively. Bone volume/tissue volume (%BV/TV) measurements include residual trabecular and remaining cortical bone for PC3 models, as well as new bone formation in the bone marrow cavity in the PC3c model. Tibiae from animals were fixed, decalcified in Osteosoft® (Merck, Darmstadt, Germany) for four weeks, and then embedded in paraffin. In order to calculate the tumor burden to soft tissue volume (TB/STV) ratio (i.e., percentage of tumor tissue), sections of 5 μm were stained with Goldner's trichrome and histomorphometric analyses were performed. The *in situ* detection of osteoclasts was carried out on metastatic bone tissue sections using the tartrate-resistant acid phosphatases (TRAP) activity assay kit (Sigma-Aldrich, Saint-Louis, MO, USA). The osteoclastic surface (OC.S/BS) was calculated as the ratio of TRAP-positive trabecular bone surface (OC.S) to the total bone surface (BS), using the computerized image system MorphoExpert (Exploranova).

2.9. Human PCa bone and lymph node metastasis samples

Human PCa bone (n=5) and lymph node (n=3) metastases were obtained from the local tumor tissue bank, C2RC (Lille, France), after the internal review board's approval (CSTMT-042, 27/07/2009). These tumor tissue samples, which had previously been extracted and subsequently frozen, originated from patients who consult at Lille University Hospitals (CHRU de Lille). Lymph node samples were obtained during radical prostatectomies or trans-urethral prostatic resections, while the bone samples were acquired during either spinal cord decompression surgery, or prosthetic placements. All patients were informed and consent was obtained by the referring physician. Pathological findings of these PCa metastasis samples can be found in Supplemental Table 2.

2.10. Immunohistochemistry

Immunohistochemistry of human and mouse tissue sections was performed using anti-ERG (ab92513, Abcam, Cambridge, UK) at 1/100, anti-Ki67 (ab15580, Abcam, Cambridge, UK) at 1/200, and anti-ET-1 (No250640, Abbiotec, San Diego, CA, USA) at 1/100. Sections were incubated with secondary HRP-conjugated antibody. Counterstaining was performed using Mayer's hematoxylin (Merck, Darmstadt, Germany). Images were acquired using an Axio Scan.Z1 slide scanner and ZEN (Blue edition) 2012 software (Carl Zeiss, Oberkochen, Germany).

2.11. Image treatment and statistical analysis

All image treatments were carried out using Image J. Statistical analyses were performed using the GraphPad Prism software (San Diego, CA, USA). The statistical methods used in this study are indicated in the corresponding figure legends. Unless otherwise indicated, all values in the figures are expressed as means ± s.e.m.

3. Results

3.1. TMPRSS2:ERG expression in PCa cells enhances osteoblastic lesions in vivo

In order to assess whether *TMPRSS2:ERG* gene fusions are involved in PCa bone metastasis progression *in vivo*, we chose to use a PCa-induced bone metastasis murine model. For this purpose we used the human *TMPRSS2:ERG*-negative PCa cell line, PC3c, which was originally derived from the PC3 cell line. We were mindful that it had been shown that the parental PC3 cells solely induce pure osteolytic bone lesions [24]. However mixed osteolytic/osteoblastic bone lesions have been found in most human PCa bone metastasis samples [6], and we therefore used the PC3c cells which are some of the rare human cell lines capable of inducing mixed osteoblastic/osteolytic bone lesions when injected into the tibiae of

male SCID mice [24]. One of the advantages was that such cells more accurately mimic the phenotype of human bone metastasis progression than any other available PCa cell lines. We had previously established and characterized several PC3c cell clones which stably expressed the most common *TMPRSS2:ERG* fusion, named T1E4. That fusion consists in the noncoding exon 1 of *TMPRSS2* fused with the coding of exons of ERG from exon 4 [19]. The forced expression of *TMPRSS2:ERG* in PC3c cells (PC3c-T1E4) resulted in an increase of their migration and invasion capacities *in vitro* of those cells. In order to avoid any single-clone cell effect we injected into the tibiae of SCID mice the PC3c cell clones expressing distinct levels (low, medium and high expression) of the TMPRSS2:ERG fusion applying a 1:1:1 ratio. A control group made up of PC3c cells expressing empty pcDNA vector (PC3c-CT) was also injected.

Ten weeks after injection, radiographical analyses revealed that, compared to the control animals, animals bearing tumors overexpressing the TMPRSS2:ERG fusion exhibited respectively significantly smaller and larger bone destruction and formation areas (Figs. 1A and 1B). We then decided to carry out additional experiments in order to be as complete and thorough as possible in our analysis. First, we used three-dimensional micro-computed tomographic reconstruction, which showed that tibiae bearing PC3c-T1E4 cells had a larger bone volume than those injected with PC3c-CT cells (Figs. 1C and 1D). Secondly, we undertook Goldner's trichrome staining of the tissue sections and a histomorphometric analysis of tibiae lesions which respectively showed that PC3c-T1E4 cell inoculation resulted in an induced bone formation within the bone marrow cavity and a lower skeletal tumor burden (Figs. 1E and 1F). Third, TRAP staining revealed 20% less TRAP-positive osteoclast surface (OC.S/BS) in tibiae injected with PC3c-T1E4 cells compared to those inoculated with control PC3c-CT cells (Figs. 1G and 1H). Finally, by means of control, the immunostaining of the bone lesions revealed the presence of Ki-67-positive proliferating tumor cells, for which ectopic expression of *ERG* was also confirmed (Fig. 1I). Collectively, these data show

that the expression of the *TMPRSS2:ERG* fusion in PC3c cells is capable of enhancing the osteoblastic phenotype of skeletal lesions.

In contrast to PC3c cells, PC3 cells are known to solely induce pure osteolytic lesions when injected into the tibiae of mice. We then hypothesized that ectopic expression of *TMPRSS2:ERG* in PC3 cells would be capable of altering bone lesion characteristics just as it did in the PC3c model. Six weeks after intratibial tumor cell injection, both the T1E4-expressing PC3 cells (PC3-T1E4) and the PC3 control cells (PC3-CT) had induced osteolytic lesions (Fig. 2A). However, the PC3-T1E4-bearing bone showed a significantly lower level of bone destruction (Fig. 2B), a larger bone volume (Figs. 2C and 2D), and a lower tumor burden (Figs. 2E and 2F). Similar to effect observed in the PC3c model, TRAP staining of tibial sections from animals bearing PC3-T1E4 cells showed 5% less TRAP-positive osteoclast surface compared to control tibiae (Figs. 2G and 2H). Cancer cells were detected in these bone lesions using Ki-67 and ERG antibody-based immunostaining (Fig. 2I). These results suggest that the expression of *TMPRSS2:ERG* in PC3 cells inhibits osteoclasts and decreases bone destruction.

Taken together, our results indicate that overexpression of the *TMPRSS2:ERG* fusion in PCa cells increases the osteoblastic phenotype of bone lesions and inhibits osteoclastic destruction *in vivo*.

3.2. TMPRSS2:ERG expression enhances osteomimicry properties of PCa cells

The acquisition of a bone cell-like phenotype, namely osteomimicry, has been proposed to help cancer cells survive within the bone microenvironment [2, 5]. For instance, it has been shown that PCa cells can overexpress factors responsible for osteoblast differentiation and bone matrix mineralization [4]. Specifically, PC3c cells have been shown to express bone-associated markers such as *OPN* (*Osteopontin*), *BSP* (*Bone Sialoprotein*), *RUNX2* (*Runt Related Transcription Factor 2*) and *COL1A1* (*Collagen Type I Alpha 1*

Chain), which allow them to form a calcified matrix under osteogenic conditions [24]. As ectopic expression of the *TMPRSS2:ERG* fusion gene in PC3c cells enhanced osteoblastic lesion formation, we contemplated whether this aberrant ERG expression could have an impact on the osteomimicry properties of PC3c cells. Indeed, after 3 weeks of culture in osteogenic conditions, including ascorbic acid and β-glycerophosphate, PC3c-T1E4 cells showed some mineralization (black zones) and a higher ALPL *(*Alkaline Phosphatase, Liver/Bone/Kidney) activity than control PC3c-CT cells (in pink) (Fig. 3A). Although the expression levels of *BSP* and *OCN* (*Osteocalcin*) were comparable between PC3c-T1E4 and PC3c-CT cells (Fig. 3B), in PC3c-T1E4 cells there was a higher expression of the early osteoblast differentiation marker *ALPL*, as well as of *COL1A1* and *OPN,* two genes associated with crucial organic bone matrix components (Fig. 3B). In addition, we found that the expression of *OPG* (*Osteoprotegerin*), which is known to inhibit osteoclastogenesis by interacting with RANKL (Receptor Activator of Nuclear Factor Kappa-B Ligand), was also higher in PC3c-T1E4 cells (Fig. 3B). Moreover, this osteomimicry enhancement was also observed, albeit to a lesser extent, in PC3-T1E4 cells cultured under osteogenic conditions (Figs. 3C and 3D). Interestingly *RANKL* expression was down-regulated in PC3-T1E4 cells.

To further confirm the clinical relevance of this regulatory network, we analyzed a gene expression dataset based on 52 human prostate adenocarcinoma metastasis samples using the cBioPortal platform [25]. Indeed, due to the difficulty to obtain metastasis samples, particularly bone metastases, very few cohorts have been studied. In this cohort, we found that the expression levels of the potential novel targets *ALPL* and *COL1A1*, are indeed significantly correlated with the expression of *ERG* (Fig. 4). In addition, a correlated expression also exists between *ERG* and the other bone remodeling-associated marker, *OPN* (Fig. 4). Importantly, *OPN* has previously been shown to be a target gene of ERG in PCa [32], and has a documented role in osteoblastic lesion formation induced by cancer cells [33]. On the other hand, no correlations were observed with *BSP*, *OCN*, *OPG* or *RANKL*. Such clinical

relevance further highlights the importance of the ERG transcription factor in the control of a bone turnover-associated gene network *in vivo*.

These data suggest that the expression of the *TMPRSS2:ERG* fusion in PCa cells enhances their osteomimicry properties, thereby explaining, at least in part, their capacity to increase the osteoblastic response *in vivo*.

3.3. ERG directly controls the expression of ALPL and COL1A1 in PCa cells

Our results demonstrate that aberrant expression of ERG in PCa cells can enhance their osteomimicry properties through increasing osteogenic marker expression. We therefore asked whether these osteogenic markers are directly regulated by ERG in PCa cells. We took advantage of the availability of published ERG ChIP-seq data performed in the VCaP cell line, which is the only cell line harboring endogenous expression of TMPRSS2:ERG [34], to perform analyses showing that ERG binds to active regulatory regions of the *ALPL* and *COL1A1* genes (Figs. S1 and S2) [21, 28, 29]. Moreover, these genomic regions correspond to transcriptionaly active regions since they were marked by the active transcriptional regulatory epigenetic marks H3K4me1 (histone 3 lysine 4 monomethylation), H3K4me3 (histone 3 lysine 4 trimethylation), H3K27ac (histone 3 lysine 27 acetylation) or DNaseI sensitivity clusters. Importantly, knockdown of *TMPRSS2:ERG* fusion expression in VCaP cells (Fig. 5A) significantly decreased the expression of *ALPL* and *COL1A1* by 27% and 58%, respectively (Figs. 5B and 5C). In contrast, when the same cells were treated with DHT to increase *TMPRSS2:ERG* fusion expression (Fig. 5D), there was a significant increase in the expression levels of *ALPL* (four-fold) and *COL1A1* (seven-fold) (Figs. 5E and 5F).

Furthermore, we also found that ectopic expression of the fusion in PC3c cells (Fig. 5G) resulted in an increased expression of both *ALPL* and *COL1A1* (three-fold and two-fold, respectively) even though cell cultures were performed without osteogenic conditions (Figs. 5H and 5I). This *ALPL* and *COL1A1* upregulation was specific to ectopic expression of ERG

because silencing the *TMPRSS2:ERG* fusion in PC3c-T1E4 cells (Fig. 5J) led to a reduced expression of both osteogenic markers (Figs. 5K and 5L). Likewise, in PC3c-T1E4 cells, we also found that ERG significantly binds to the same regulatory regions of *ALPL* and *COL1A1* that were identified in VCaP cells (Figs. 5M and 5N).

These results demonstrate that ERG directly controls the expression of the *ALPL* and *COL1A1* osteogenic markers in PCa cells.

3.4. ERG transcription factor regulates ET-1 expression in PCa cells

To further understand the mechanism by which aberrant expression of *TMPRSS2:ERG* fusions in PCa cells contributes to osteoblastic lesion formation, we focused on gene expression comparisons between the PC3c-CT and PC3c–T1E4 cell clones obtained previously [19]. Interestingly, in cells expressing *TMPRSS2:ERG*, the expression of *ET-1* is upregulated. The *ET-1* gene encodes a 21-amino acid secreted peptide that has a documented role in osteoblastic lesion formation in PCa bone metastases [35]. In fact, this peptide is able to stimulate osteoblast differentiation [36] and prevent osteoclast-mediated bone resorption [37, 38], thereby promoting overall osteoblastic lesion formation. Moreover, using the cBioPortal platform to analyze the gene expression dataset based on 52 human prostate adenocarcinoma metastasis samples, we found that the expression levels of this *ET-1* gene was also significantly correlated with the expression of ERG (Fig. 4).

By using PC3c clones expressing distinct levels of the *TMPRSS2:ERG* T1E4 fusion (low, medium and high), we first confirmed that forced expression of the fusion results in *ET-1* upregulation. In fact, the increase in *ET-1* mRNA levels was correlated with the expression level of the fusion (Fig. 5G and 6A). In agreement with these results, an ELISA assay revealed that PC3c-T1E4 clones secreted significantly higher levels of ET-1 compared to control PC3c-CT cells (Fig. 6B). Importantly, knocking down expression of the *TMPRSS2:ERG* fusion in PC3c-T1E4 cells using an siRNA against *ERG*, led to

approximately a 40% reduction in *ET-1* expression compared to in control siRNA-transfected cells (Fig. 5J and 6C). In addition, to further test the possible role of TMPRSS2:ERG in regulating *ET-1* expression, we used another PCa cell line, VCaP, harboring endogenous expression of TMPRSS2:ERG. Knocking down the *TMPRSS2:ERG* fusion in VCaP cells resulted in a significant decrease in *ET-1* expression (40%; Fig. 5A and 6D). Furthermore, DHT-stimulated *TMPRSS2:ERG* fusion expression was associated with a significant increase in *ET-1* mRNA expression (Fig. 5D and 6E). Interestingly, using published ERG ChIP-seq data [21, 28, 29] obtained from VCaP cells, we found that there are three ERG binding sites at the *ET-1* gene locus (Fig. S3). Moreover, these sites were modulated by hormonal induction and marked by the active transcriptional regulatory epigenetic marks. As such, we performed ChIP-qPCR assays and also found significant ERG binding to these regulatory elements in PC3c-T1E4 cells (Figs. 6F-H). Taken together, our results highlight that ERG, which becomes aberrantly expressed due to the *TMPRSS2:ERG* rearrangement, directly controls *ET-1* expression in PCa cells.

To verify whether ERG is capable of regulating *ET-1* gene expression in human metastasis samples, we performed immune-detection in human samples. We used ERG and ET-1 immunohistochemistry staining in fusion-positive and –negative human lymph node and bone metastasis samples. As expected, ERG expression was strong in fusion-positive metastatic tissues, but was restricted to the endothelial cells of blood vessels in fusion-negative (Fig. 7). Moreover, while ET-1 was barely detected in lymph node metastases, a strong expression of ET-1 was detected in fusion-positive bone metastasis tissues (Fig. 7).

Together, these results reveal a link between ERG and ET-1 expression in fusion-positive human bone metastasis samples.

4. Discussion

PCa cells most commonly metastasize to the bone, inducing osteoblastic or mixed osteoblastic/osteolytic lesions, and this is an incurable complication of the disease [1, 6]. In the present study, we demonstrate that the *TMPRSS2:ERG* fusion is involved in bone metastasis phenotype by influencing the critical interplay between PCa cells and the bone microenvironment. Using a murine intratibial PCa engraftment model, we found that ectopic expression of the *TMPRSS2:ERG* fusion in PC3c or PC3 cells, which are known to induce mixed osteoblastic/osteolytic or solely pure osteolytic lesions respectively [24], results in an increase in bone formation events and a decrease in bone resorption. Since bone homeostasis is tightly controlled by the balance between osteoclast and osteoblast activities [2, 7, 39], our results suggest that PCa cells harboring the *TMPRSS2:ERG* fusion are able to interrupt this balance in favor of osteoblastic activity.

Indeed, we found that, in PCa cells, the ERG transcription factor is capable of directly controlling the expression of major bone markers, such as *ALPL* and *COL1A1* [40, 41]. By enhancing the expression of *ALPL* and *COL1A1* in tumor cells, ERG promotes the osteomimicry properties of the tumor cells, likely facilitating their survival and growth in the bone microenvironment. Importantly, ALPL and COL1A1 directly participate in the bone formation process [2, 7]: ALPL, a pivotal early marker of osteoblast activity, has been shown as essential for matrix mineralization and COL1A1, which is mainly secreted by osteoblasts, makes up approximately 90% of the bone matrix [42, 43]. Noteworthy, among the bone-related parameters detected in patient blood, the level of ALPL has been identified as an important predictor of bone metastases [44, 45]. Recently, it has been shown that ALPL may be a major contributor to the progression of PCa, and that ALPL reduction increases cell death and epithelial plasticity in PCa cells [46]. In addition to the *ALPL* and *COL1A1* genes, we have previously shown that ERG also controls the expression of *OPN* [32], another gene involved in the bone remodeling and mineralization processes. Thus, one of the principal consequences of the aberrant expression of TMPRSS2:ERG in PCa cells is a conferred bone-

like phenotype. This not only enhances bone formation, but is also the underlying cause that provides PCa cells with a survival advantage in the bone microenvironment.

Here, we also found the *ET-1* gene to be a direct target of ERG in PCa cells. Importantly, *ET-1* expression was also significantly associated with ERG expression in human metastasis samples. The *ET-1* gene encodes a secreted peptide that is known to promote osteoblastic bone lesions during metastatic growth of prostate tumors in mouse models [40]. Moreover, higher concentrations of ET-1 have been found in the plasma of metastatic PCa patients [47]. In fact, ET-1 is known to exert paracrine and autocrine effects by binding to the ET-1 receptors A and B, ETAR and ETBR [41]. Activation of ETAR by ET-1 can promote PCa growth through pathways involved in angiogenesis, osteogenesis, cell migration and invasion [48]. This suggests that the ET-1 axis could be an attractive therapeutic target for inhibiting cancer growth and metastasis. Clinical trials have shown that ETAR antagonists such as atrasentan (ABT-627, Abbott Laboratories, Abbott Park, CA, USA) and zibotentan (ZD4054, Astra-Zeneca, London, UK), result in a delay in skeletal metastasis progression, a decrease in cancer-related bone pain, and an increase in the overall survival of patients with castration-resistant PCa and bone metastases [49, 50]. However, despite promising Phase II trials in patients with advanced metastatic PCa, Phase III trials using atrasentan and zibotentan mono-therapy or in combination with docetaxel chemotherapy, were unsuccessful in patients with established disease [51, 52]. Two possible reasons for these clinical findings could be that the dose of chemotherapy received by the patients was too weak or, more importantly, that screening patients for non-metastatic disease status can prove difficult [52]. As patients with highly elevated bone turnover markers appear to preferentially benefit from atrasentan therapy [53], TMPRSS2:ERG-positive or -negative fusion levels, which we show to be associated with bone marker levels, could help in selecting good responders for ETAR treatment in further Phase III trials.

The formation of metastasis is a multistep process that includes dissemination of cancer cells from primary tumor, organotropism (i.e. bone tropism) and tissue colonization, survival and dormancy of the tumor cells, and finally, after dormant state escape, uncontrollably proliferation [2, 7]. In PCa, TMPRSS2:ERG fusions are found in more than a half of cases, and bone is the primary site of metastasis. However, only one cell line, VCaP, exhibits the endogenous TMPRSS2:ERG fusion, very few cell lines are able to induce lesions in bone, and none of the existing mouse models entirely recapitulate the metastatic processes [34, 54]. Such limitation constitutes a limit to the understanding of bone metastasis formation itself.

Nonetheless, PC3 represent an appropriate widely used cell model to study the specific role of TMPRSS2:ERG in the phenotype of induced bone lesions. Indeed, this cell line was produced from a PCa bone metastasis, was free from any chromosomic rearrangements or fusion genes, especially TMPRSS2:ERG, and was known to induce pure osteolytic lesions in murine intratibial PCa engraftment models. Using three PC3-derived cell lines, we showed that the *TMPRSS2:ERG* fusion gene expression contributes to at least two steps of this process: first, the bone tropism as shown by our previously-described intracardiac injection experiments [23], and second, the development of osteoblastic lesion presented in this study. These intracardiac and intratibial injection models highlight distinct series of genes, regulated by the TMPRSS2:ERG proteins. Associated to cell adhesion and migration [23], or to bone cell differentiation and mineralization as identified here, these genes respectively contributed to these two steps of bone metastasis formation. It will be important in future work to assess the contribution of TMPRSS2:ERG in additional models of PCa that could include the use of transgenic mouse models or primary patient samples as Patient-Derived Xenografts.

In conclusion, our study provides both *in vivo* and *in vitro* evidence supporting that aberrant expression of the *TMPRSS2:ERG* fusion in PCa cells enhances their osteomimicry and promotes osteoblastic lesion formation. Therefore, in addition to the presence of the

fusion, the detection of ALPL, COL1A1 and ET-1 protein expressions could constitute a signature which indicates the metastatic progression and provide a novel tool for the assessment, treatment and management of patients with PCa.

Grant supports

This work was in part supported by the Centre national de la recherche scientifique (CNRS) ; Ligue nationale contre le Cancer (Comité du Pas-de-Calais) ; Institut national du cancer (INCa_4419) ; Institut Pasteur de Lille, Conseil Régional du Nord-Pas-de-Calais and Fondation pour la Recherche Médicale (FRM) ; Conseil Régional du Nord-Pas-de-Calais ; Association pour la Recherche sur le Cancer (ARC) ; MINECO (Juan de la Cierva Postdoctoral Fellowship FJCI-2014-22946) ; ARTP (Association de Recherche sur les tumeurs de prostate).

Acknowledgments

We would like to thank M. Tardivel, A. Bongiovanni and E. Werkmeister from the BioImaging Center Lille Nord de France (BICeL) for their technical assistance; M. Canouil for his statistics advice; and M. Vernier for his bioinformatics advice and stimulating discussions. We would also like to thank the local Tumor Tissue Bank (Tumorothèque), Regional Reference Oncology Center (CRRC) (Head, Pr. M.C. Copin) in Lille, France.

Conflict of interest

All authors declare no conflict of interest.

References

[1] G.R. Mundy, Metastasis to bone: causes, consequences and therapeutic opportunities, Nat Rev Cancer 2 (2002) 584-593.

[2] C. Kan, G. Vargas, F.L. Pape, P. Clezardin, Cancer Cell Colonisation in the Bone Microenvironment, Int J Mol Sci 17 (2016) 1674.

[3] T. Ibrahim, E. Flamini, L. Mercatali, E. Sacanna, P. Serra, D. Amadori, Pathogenesis of osteoblastic bone metastases from prostate cancer, Cancer 116 (2010) 1406-1418.

[4] K.S. Koeneman, F. Yeung, L.W. Chung, Osteomimetic properties of prostate cancer cells: a hypothesis supporting the predilection of prostate cancer metastasis and growth in the bone environment, Prostate 39 (1999) 246-261.

[5] K.N. Weilbaecher, T.A. Guise, L.K. McCauley, Cancer to bone: a fatal attraction, Nat Rev Cancer 11 (2011) 411-425.

[6] C.J. Logothetis, S.H. Lin, Osteoblasts in prostate cancer metastasis to bone, Nat Rev Cancer 5 (2005) 21-28.

[7] P.I. Croucher, M.M. McDonald, T.J. Martin, Bone metastasis: the importance of the neighbourhood, Nat Rev Cancer 16 (2016) 373-386.

[8] L.A. Kingsley, P.G. Fournier, J.M. Chirgwin, T.A. Guise, Molecular biology of bone metastasis, Mol Cancer Ther 6 (2007) 2609-2617.

[9] S.A. Tomlins, D.R. Rhodes, S. Perner, S.M. Dhanasekaran, R. Mehra, X.W. Sun, S. Varambally, X. Cao, J. Tchinda, R. Kuefer, C. Lee, J.E. Montie, R.B. Shah, K.J. Pienta, M.A. Rubin, A.M. Chinnaiyan, Recurrent fusion of TMPRSS2 and ETS transcription factor genes in prostate cancer, Science 310 (2005) 644-648.

[10] M.A. Rubin, C.A. Maher, A.M. Chinnaiyan, Common gene rearrangements in prostate cancer, J Clin Oncol 29 (2011) 3659-3668.

[11] A.B. Rajput, M.A. Miller, A. De Luca, N. Boyd, S. Leung, A. Hurtado-Coll, L. Fazli, E.C. Jones, J.B. Palmer, M.E. Gleave, M.E. Cox, D.G. Huntsman, Frequency of the TMPRSS2:ERG gene fusion is increased in moderate to poorly differentiated prostate cancers, J Clin Pathol 60 (2007) 1238-1243.

[12] F. Demichelis, K. Fall, S. Perner, O. Andren, F. Schmidt, S.R. Setlur, Y. Hoshida, J.M. Mosquera, Y. Pawitan, C. Lee, H.O. Adami, L.A. Mucci, P.W. Kantoff, S.O. Andersson, A.M. Chinnaiyan, J.E. Johansson, M.A. Rubin, TMPRSS2:ERG gene fusion associated with lethal prostate cancer in a watchful waiting cohort, Oncogene 26 (2007) 4596-4599.

[13] R.M. Hagen, P. Adamo, S. Karamat, J. Oxley, J.J. Aning, D. Gillatt, R. Persad, M.R. Ladomery, A. Rhodes, Quantitative analysis of ERG expression and its splice isoforms in formalin-fixed, paraffin-embedded prostate cancer samples: association with seminal vesicle invasion and biochemical recurrence, Am J Clin Pathol 142 (2014) 533-540.

[14] R.K. Nam, L. Sugar, W. Yang, S. Srivastava, L.H. Klotz, L.Y. Yang, A. Stanimirovic, E. Encioiu, M. Neill, D.A. Loblaw, J. Trachtenberg, S.A. Narod, A. Seth, Expression of the TMPRSS2:ERG fusion gene predicts cancer recurrence after surgery for localised prostate cancer, Br J Cancer 97 (2007) 1690-1695.

[15] P. Adamo, M.R. Ladomery, The oncogene ERG: a key factor in prostate cancer, Oncogene 35 (2016) 403-414.

[16] A. Gopalan, M.A. Leversha, J.M. Satagopan, Q. Zhou, H.A. Al-Ahmadie, S.W. Fine, J.A. Eastham, P.T. Scardino, H.I. Scher, S.K. Tickoo, V.E. Reuter, W.L. Gerald, TMPRSS2-ERG gene fusion is not associated with outcome in patients treated by prostatectomy, Cancer Res 69 (2009) 1400-1406.

[17] B.S. Carver, J. Tran, A. Gopalan, Z. Chen, S. Shaikh, A. Carracedo, A. Alimonti, C. Nardella, S. Varmeh, P.T. Scardino, C. Cordon-Cardo, W. Gerald, P.P. Pandolfi, Aberrant ERG expression cooperates with loss of PTEN to promote cancer progression in the prostate, Nat Genet 41 (2009) 619-624.

[18] S.A. Tomlins, B. Laxman, S. Varambally, X. Cao, J. Yu, B.E. Helgeson, Q. Cao, J.R. Prensner, M.A. Rubin, R.B. Shah, R. Mehra, A.M. Chinnaiyan, Role of the TMPRSS2-ERG gene fusion in prostate cancer, Neoplasia 10 (2008) 177-188.

[19] T.V. Tian, N. Tomavo, L. Huot, A. Flourens, E. Bonnelye, S. Flajollet, D. Hot, X. Leroy, Y. de Launoit, M. Duterque-Coquillaud, Identification of novel TMPRSS2:ERG mechanisms in prostate cancer metastasis: involvement of MMP9 and PLXNA2, Oncogene 33 (2014) 2204-2214.

[20] P.C. Hollenhorst, M.W. Ferris, M.A. Hull, H. Chae, S. Kim, B.J. Graves, Oncogenic ETS proteins mimic activated RAS/MAPK signaling in prostate cells, Genes Dev 25 (2011) 2147-2157.

[21] K.R. Chng, C.W. Chang, S.K. Tan, C. Yang, S.Z. Hong, N.Y. Sng, E. Cheung, A transcriptional repressor co-regulatory network governing androgen response in prostate cancers, EMBO J 31 (2012) 2810-2823.

[22] J. Yu, J. Yu, R.S. Mani, Q. Cao, C.J. Brenner, X. Cao, X. Wang, L. Wu, J. Li, M. Hu, Y. Gong, H. Cheng, B. Laxman, A. Vellaichamy, S. Shankar, Y. Li, S.M. Dhanasekaran, R. Morey, T. Barrette, R.J. Lonigro, S.A. Tomlins, S. Varambally, Z.S. Qin, A.M. Chinnaiyan, An integrated network of androgen receptor, polycomb, and TMPRSS2-ERG gene fusions in prostate cancer progression, Cancer Cell 17 (2010) 443-454.

[23] R. Deplus, C. Delliaux, N. Marchand, A. Flourens, N. Vanpouille, X. Leroy, Y. de Launoit, M. Duterque-Coquillaud, TMPRSS2-ERG fusion promotes prostate cancer metastases in bone, Oncotarget 8 (2017) 11827-11840.

[24] A. Fradet, H. Sorel, B. Depalle, C.M. Serre, D. Farlay, A. Turtoi, A. Bellahcene, H. Follet, V. Castronovo, P. Clezardin, E. Bonnelye, A new murine model of osteoblastic/osteolytic lesions from human androgen-resistant prostate cancer, PLoS One 8 (2013) e75092.

[25] H. Beltran, D. Prandi, J.M. Mosquera, M. Benelli, L. Puca, J. Cyrta, C. Marotz, E. Giannopoulou, B.V. Chakravarthi, S. Varambally, S.A. Tomlins, D.M. Nanus, S.T. Tagawa, E.M. Van Allen, O. Elemento, A. Sboner, L.A. Garraway, M.A. Rubin, F. Demichelis,

Divergent clonal evolution of castration-resistant neuroendocrine prostate cancer, Nat Med 22 (2016) 298-305.

[26] E. Cerami, J. Gao, U. Dogrusoz, B.E. Gross, S.O. Sumer, B.A. Aksoy, A. Jacobsen, C.J. Byrne, M.L. Heuer, E. Larsson, Y. Antipin, B. Reva, A.P. Goldberg, C. Sander, N. Schultz, The cBio cancer genomics portal: an open platform for exploring multidimensional cancer genomics data, Cancer Discov 2 (2012) 401-404.

[27] J. Gao, B.A. Aksoy, U. Dogrusoz, G. Dresdner, B. Gross, S.O. Sumer, Y. Sun, A. Jacobsen, R. Sinha, E. Larsson, E. Cerami, C. Sander, N. Schultz, Integrative analysis of complex cancer genomics and clinical profiles using the cBioPortal, Sci Signal 6 (2013) pl1.

[28] I.A. Asangani, V.L. Dommeti, X. Wang, R. Malik, M. Cieslik, R. Yang, J. Escara-Wilke, K. Wilder-Romans, S. Dhanireddy, C. Engelke, M.K. Iyer, X. Jing, Y.M. Wu, X. Cao, Z.S. Qin, S. Wang, F.Y. Feng, A.M. Chinnaiyan, Therapeutic targeting of BET bromodomain proteins in castration-resistant prostate cancer, Nature 510 (2014) 278-282.

[29] N.L. Sharma, C.E. Massie, F. Butter, M. Mann, H. Bon, A. Ramos-Montoya, S. Menon, R. Stark, A.D. Lamb, H.E. Scott, A.Y. Warren, D.E. Neal, I.G. Mills, The ETS family member GABPalpha modulates androgen receptor signalling and mediates an aggressive phenotype in prostate cancer, Nucleic Acids Res 42 (2014) 6256-6269.

[30] S. Mei, Q. Qin, Q. Wu, H. Sun, R. Zheng, C. Zang, M. Zhu, J. Wu, X. Shi, L. Taing, T. Liu, M. Brown, C.A. Meyer, X.S. Liu, Cistrome Data Browser: a data portal for ChIP-Seq and chromatin accessibility data in human and mouse, Nucleic Acids Res 45 (2017) D658-D662.

[31] W.J. Kent, C.W. Sugnet, T.S. Furey, K.M. Roskin, T.H. Pringle, A.M. Zahler, D. Haussler, The human genome browser at UCSC, Genome Res 12 (2002) 996-1006.

[32] S. Flajollet, T.V. Tian, A. Flourens, N. Tomavo, A. Villers, E. Bonnelye, S. Aubert, X. Leroy, M. Duterque-Coquillaud, Abnormal expression of the ERG transcription factor in prostate cancer cells activates osteopontin, Mol Cancer Res 9 (2011) 914-924.

[33] T.E. Kruger, A.H. Miller, A.K. Godwin, J. Wang, Bone sialoprotein and osteopontin in bone metastasis of osteotropic cancers, Crit Rev Oncol Hematol 89 (2014) 330-341.

[34] S. Korenchuk, J.E. Lehr, M.C. L, Y.G. Lee, S. Whitney, R. Vessella, D.L. Lin, K.J. Pienta, VCaP, a cell-based model system of human prostate cancer, In Vivo 15 (2001) 163-168.

[35] J.J. Yin, K.S. Mohammad, S.M. Kakonen, S. Harris, J.R. Wu-Wong, J.L. Wessale, R.J. Padley, I.R. Garrett, J.M. Chirgwin, T.A. Guise, A causal role for endothelin-1 in the pathogenesis of osteoblastic bone metastases, Proc Natl Acad Sci U S A 100 (2003) 10954-10959.

[36] K. Suzuki, K. Aoki, K. Ohya, Effects of surface roughness of titanium implants on bone remodeling activity of femur in rabbits, Bone 21 (1997) 507-514.

[37] A.S. Alam, A. Gallagher, V. Shankar, M.A. Ghatei, H.K. Datta, C.L. Huang, B.S. Moonga, T.J. Chambers, S.R. Bloom, M. Zaidi, Endothelin inhibits osteoclastic bone resorption by a direct effect on cell motility: implications for the vascular control of bone resorption, Endocrinology 130 (1992) 3617-3624.

[38] J.W. Chiao, B.S. Moonga, Y.M. Yang, R. Kancherla, A. Mittelman, J.R. Wu-Wong, T. Ahmed, Endothelin-1 from prostate cancer cells is enhanced by bone contact which blocks osteoclastic bone resorption, Br J Cancer 83 (2000) 360-365.

[39] T.A. Guise, K.S. Mohammad, G. Clines, E.G. Stebbins, D.H. Wong, L.S. Higgins, R. Vessella, E. Corey, S. Padalecki, L. Suva, J.M. Chirgwin, Basic mechanisms responsible for osteolytic and osteoblastic bone metastases, Clin Cancer Res 12 (2006) 6213s-6216s.

[40] T.A. Guise, J.J. Yin, K.S. Mohammad, Role of endothelin-1 in osteoblastic bone metastases, Cancer 97 (2003) 779-784.

[41] L. Rosano, F. Spinella, A. Bagnato, Endothelin 1 in cancer: biological implications and therapeutic opportunities, Nat Rev Cancer 13 (2013) 637-651.

[42] K.G. Waymire, J.D. Mahuren, J.M. Jaje, T.R. Guilarte, S.P. Coburn, G.R. MacGregor, Mice lacking tissue non-specific alkaline phosphatase die from seizures due to defective metabolism of vitamin B-6, Nat Genet 11 (1995) 45-51.

[43] K.N. Fedde, L. Blair, J. Silverstein, S.P. Coburn, L.M. Ryan, R.S. Weinstein, K. Waymire, S. Narisawa, J.L. Millan, G.R. MacGregor, M.P. Whyte, Alkaline phosphatase knock-out mice recapitulate the metabolic and skeletal defects of infantile hypophosphatasia, J Bone Miner Res 14 (1999) 2015-2026.

[44] V. Pasoglou, N. Michoux, F. Peeters, A. Larbi, B. Tombal, T. Selleslagh, P. Omoumi, B.C. Vande Berg, F.E. Lecouvet, Whole-body 3D T1-weighted MR imaging in patients with prostate cancer: feasibility and evaluation in screening for metastatic disease, Radiology 275 (2015) 155-166.

[45] A.R. Metwalli, I.L. Rosner, J. Cullen, Y. Chen, T. Brand, S.A. Brassell, J. Lesperance, C. Porter, J. Sterbis, D.G. McLeod, Elevated alkaline phosphatase velocity strongly predicts overall survival and the risk of bone metastases in castrate-resistant prostate cancer, Urol Oncol 32 (2014) 761-768.

[46] S.R. Rao, A.E. Snaith, D. Marino, X. Cheng, S.T. Lwin, I.R. Orriss, F.C. Hamdy, C.M. Edwards, Tumour-derived alkaline phosphatase regulates tumour growth, epithelial plasticity and disease-free survival in metastatic prostate cancer, Br J Cancer 116 (2017) 227-236.

[47] J.B. Nelson, S.H. Nguyen, J.R. Wu-Wong, T.J. Opgenorth, D.B. Dixon, L.W. Chung, N. Inoue, New bone formation in an osteoblastic tumor model is increased by endothelin-1 overexpression and decreased by endothelin A receptor blockade, Urology 53 (1999) 1063-1069.

[48] A. Bagnato, M. Loizidou, B.R. Pflug, J. Curwen, J. Growcott, Role of the endothelin axis and its antagonists in the treatment of cancer, Br J Pharmacol 163 (2011) 220-233.

[49] N.D. James, A. Caty, H. Payne, M. Borre, B.A. Zonnenberg, P. Beuzeboc, S. McIntosh, T. Morris, D. Phung, N.A. Dawson, Final safety and efficacy analysis of the specific

endothelin A receptor antagonist zibotentan (ZD4054) in patients with metastatic castration-resistant prostate cancer and bone metastases who were pain-free or mildly symptomatic for pain: a double-blind, placebo-controlled, randomized Phase II trial, BJU Int 106 (2010) 966-973.

[50] L. Qiao, Y. Liang, N. Li, X. Hu, D. Luo, J. Gu, Y. Lu, Q. Zheng, Endothelin-A receptor antagonists in prostate cancer treatment-a meta-analysis, Int J Clin Exp Med 8 (2015) 3465-3473.

[51] K. Miller, J.W. Moul, M. Gleave, K. Fizazi, J.B. Nelson, T. Morris, F.E. Nathan, S. McIntosh, K. Pemberton, C.S. Higano, Phase III, randomized, placebo-controlled study of once-daily oral zibotentan (ZD4054) in patients with non-metastatic castration-resistant prostate cancer, Prostate Cancer Prostatic Dis 16 (2013) 187-192.

[52] E.Y. Yu, K. Miller, J. Nelson, M. Gleave, K. Fizazi, J.W. Moul, F.E. Nathan, C.S. Higano, Detection of previously unidentified metastatic disease as a leading cause of screening failure in a phase III trial of zibotentan versus placebo in patients with nonmetastatic, castration resistant prostate cancer, J Urol 188 (2012) 103-109.

[53] P.N. Lara, Jr., B. Ely, D.I. Quinn, P.C. Mack, C. Tangen, E. Gertz, P.W. Twardowski, A. Goldkorn, M. Hussain, N.J. Vogelzang, I.M. Thompson, M.D. Van Loan, Serum biomarkers of bone metabolism in castration-resistant prostate cancer patients with skeletal metastases: results from SWOG 0421, J Natl Cancer Inst 106 (2014) dju013.

[54] A.H. Jinnah, B.C. Zacks, C.U. Gwam, B.A. Kerr, Emerging and Established Models of Bone Metastasis, Cancers (Basel) 10 (2018)

Figure legends

Fig. 1. The expression of TMPRSS2:ERG in PC3c cells enhances their capacity to induce osteoformation and to reduce osteolysis. (**A**) PC3c cells expressing empty vector (PC3c-CT), T1E4 (PC3c-T1E4) and PBS buffer (Sham) were injected into the tibiae of SCID

mice. Ten weeks´ post-inoculation, radiography revealed larger osteoblastic lesions (white arrows) in mice injected with PC3c-T1E4 cells compared to those injected with PC3c-CT cells. PC3c-CT-injected mice showed both osteoblastic lesions and osteolytic destructions (white asterisks). Multiple mice of each group were analyzed, and representative radiographies are shown. (**B**) Comparison of bone destruction area (left panel; n=8, P=0.0048) and bone formation area (right panel; n=8, P=0.0032). Two-tailed Mann-Whitney t test. (**C**) 3D micro-CT reconstructions of tibiae implanted with PC3c-CT or PC3c-T1E4 cells and PBS buffer (Sham). Multiple mice of each group were analyzed, and representative radiographies are shown. (**D**) Comparison of bone volume over total tissue volume (BV/TV, %) between tibiae bearing PC3c-CT or PC3c-T1E4 cells (n=8, P=0.0207, two-tailed Mann-Whitney t test). (**E**) Goldner's trichrome staining of bone sections. Multiple mice of each group were analyzed, and representative images are shown. (**F**) Comparison of tumor burden over total soft tissue volume (TB/STV, %) between tibiae bearing PC3c-CT or PC3c-T1E4 cells (n=8, P=NS, two-tailed Mann-Whitney t test). (**G**) TRAP staining of tibiae. Six mice of each group were analyzed, and representative images are shown. (**H**) Comparison of osteoclast surface over bone surface (OC.S/BS, %) between tibiae bearing PC3c-CT or PC3c-T1E4 cells (n=6, P=0.0125, two-tailed unpaired t test). (**I**) Immunohistochemistry detection of Ki67 and ERG in tumors induced by PC3c-CT and PC3c-T1E4 cells. T, Tumor; BM, Bone Matrix; OC, Osteoclasts; GP, Growth Plate.

Fig. 2. The expression of TMPRSS2:ERG in PC3 cells enhances their capacity to reduce osteolysis. (**A**) PC3 cells expressing empty vector (PC3-CT) and T1E4 (PC3-T1E4) were injected into the tibiae of SCID mice. Four weeks´ post-inoculation, radiography revealed smaller osteolytic lesions (white asterisks) in mice injected with PC3-T1E4 cells compared to those injected with PC3-CT cells. Multiple mice of each group were analyzed, and representative radiographies are shown. (**B**) Comparison of bone destruction area (PC3-CT:

n=10, PC3-T1E4: n=11, P=0.0142, two-tailed Mann-Whitney t test). (**C**) 3D micro-CT reconstructions of tibiae implanted respectively with PC3-CT and PC3-T1E4 cells. Multiple mice of each group were analyzed, and representative radiographies are shown. (**D**) Comparison of bone volume over total tissue volume (BV/TV, %) between tibiae bearing PC3-CT or PC3-T1E4 cells (PC3-CT: n=10, PC3-T1E4: n=11, P=0.0400, two-tailed Mann-Whitney t test). (**E**) Goldner's trichrome staining of bone sections from tibiae injected with PC3-CT or PC3-T1E4. Multiple mice of each group were analyzed, and representative radiographies are shown. (**F**) Comparison of tumor burden over total soft tissue volume (TB/STV, %) between tibiae bearing PC3-CT or PC3-T1E4 cells (PC3-CT: n=10, PC3-T1E4: n=11, P=0.0016, two-tailed Mann-Whitney t test). (**G**) TRAP staining of tibiae bearing PC3-CT or PC3-T1E4 cells. Five mice of each group were analyzed, and representative images are shown. (**H**) Comparison of osteoclast surface over bone surface (OC.S/BS, %) between tibiae bearing PC3-CT or PC3-T1E4 cells (n=5, P=0.0496, two-tailed unpaired t test). (**I**) Immunohistochemistry detection of Ki67 and ERG in tumors induced by PC3-CT and PC3-T1E4 cells. T, Tumor; BM, Bone Matrix; OC, Osteoclasts; GP, Growth Plate.

Fig. 3. The expression of the TMPRSS2:ERG fusion enhances osteomimicry properties of PCa cells. (**A** and **C**) Von Kossa staining was performed on control PC3c-CT and PC3c-T1E4 cells (**A**) and on control PC3-CT and PC3-T1E4 cells (**C**) both of which were cultured in osteogenic conditions for 21 days. Von Kossa staining shows mineralization (black zones) and ALPL activity (in pink) (e.g., PC3c-T1E4 cells). (**B** and **D**) Comparison of the expression of the osteogenic markers *ALPL*, *COL1A1*, *OPN*, *BSP*, *OCN*, *OPG* and *RANKL* evaluated by RT-qPCR between control PC3c-CT and PC3c-T1E4 cells (**B**) and between control PC3-CT and PC3-T1E4 cells (**D**) both cultured in osteogenic conditions for 21 days (P values are indicated on each graph, two-tailed unpaired t test). Bar= 200 μM.

Fig. 4. The upregulation of *ERG* correlates with *ET-1* and the osteogenic markers, *ALPL*, *COL1A1* and *OPN*. cBioPortal platform analysis of a publicly available dataset of human castration resistant prostate adenocarcinoma metastasis samples (n=52, P<0.0001, Fisher's exact test) [25]. Each vertical lane represents one patient, and those shaded in dark-grey highlight the presence of mRNA upregulation.

Fig. 5. ERG directly controls the expression of *ALPL* and *COL1A1* in PCa cells. (**A-L**) The expression of *ERG*, *ALPL* and *COL1A1* were analyzed using RT-qPCR in fusion-positive VCaP cells treated with either control or ERG siRNA (**A**, **B** and **C** respectively) (n=3, ***P<0.001, one-way analysis of variance (ANOVA) with Dunnett's multiple comparison test), in fusion-positive VCaP cells treated with either ethanol vehicle (Veh) or dihydrotestosterone (DHT) to enhance ERG expression (**D**, **E** and **F** respectively) (n=3, P=0.0001, P<0.0001 and P=0.0251 respectively, unpaired t test), in the control PC3c-CT cells and PC3c-T1E4 cells expressing distinct levels (H: high; M: medium; L: low) of T1E4 fusion (**G**, **H** and **I** respectively) (n=3, **P<0.01 and ***P<0.001, one-way analysis of variance (ANOVA) with Dunnett's multiple comparison test), and in PC3c-T1E4-H cells treated with either control or ERG siRNA (**J**, **K** and **L** respectively) (n=3, **P<0.01 and ***P<0.001, one-way analysis of variance (ANOVA) with Dunnett's multiple comparison test). The expression levels of *ERG*, *ALPL* and *COL1A1* found in cells treated with control siRNA were normalized to 1. (**M-N**) ERG binding to the *ALPL* (**M**) and *COL1A1* (**N**) locus were analyzed using ChIP-qPCR in PC3c-T1E4-H and control PC3c-CT cells. The ERG binding sites identified in VCaP cells by ChIP-seq (as shown in **Supplemental Figure 1 and 2**) were analyzed. Non-specific rabbit-IgG antibody was used as a negative control. (n=3, ***P<0.001, one-way analysis of variance (ANOVA) with Dunnett's multiple comparison test).

Fig. 6. ERG transcription factor regulates *ET-1* gene expression in PCa. (**A**) The expression of *ET-1* was analyzed by RT-qPCR in the control PC3c-CT cells and PC3c-T1E4 cells expressing distinct levels (H: high; M: medium; L: low) of T1E4 fusion (n=3, ***P<0.001, one-way analysis of variance (ANOVA) with Dunnett's multiple comparison test). (**B**) The expression of the ET-1 protein was evaluated based on an ELISA of the conditioned media collected from the parental PC3c cells, control PC3c-CT cells and PC3c-T1E4 cells expressing distinct level (H: high; M: medium; L: low) of T1E4 fusion (n=3, ***P<0.001, one-way analysis of variance (ANOVA) with Dunnett's multiple comparison test). (**C-E**) The expression of *ET-1* was analyzed by RT-qPCR in PC3c-T1E4-H cells treated with either control or ERG siRNA (**C**) (n=3, ***P<0.001, one-way analysis of variance (ANOVA) with Dunnett's multiple comparison test), in fusion-positive VCaP cells treated with either control or ERG siRNA (**D**) (n=3, ***P<0.001, one-way analysis of variance (ANOVA) with Dunnett's multiple comparison test), and in fusion-positive VCaP cells treated with either ethanol vehicle (Veh) or dihydrotestosterone (DHT) to enhance ERG expression (**E**) (n=3, P<0.0001, unpaired t test). The expression levels of *ET-1* found in cells treated with control siRNA were normalized to 1. (**F-H**) The binding of ERG at the *ET-1* locus was analyzed using ChIP-qPCR in PC3c-T1E4-H and control PC3c-CT cells. All three ERG binding sites ((1), (2) and (3)) identified in VCaP cells by ChIP-seq (shown in **Supplemental Figure 3**) were analyzed (**F**), (**G**) and (**H**) respectively. Non-specific rabbit-IgG was used as a negative control (n=3, ***P<0.001, one-way analysis of variance (ANOVA) with Dunnett's multiple comparison test).

Fig. 7. ERG and ET-1 expression are associated in fusion-positive human bone metastasis samples. Immunohistochemistry staining using ERG or ET-1 specific antibodies in *TMPRSS2:ERG*-negative and -positive PCa bone (n=5) and lymph node (n=3) metastasis samples (Histo-pathological characterization of these samples in Supplemental Table 2).

Representative images were shown. T: Tumor cells; BV: Blood vessel; BM: Bone matrix; LT: Lymphoid tissue.

Figure legends

Fig. 1. The expression of TMPRSS2:ERG in PC3c cells enhances their capacity to induce osteoformation and to reduce osteolysis. (**A**) PC3c cells expressing empty vector (PC3c-CT), T1E4 (PC3c-T1E4) and PBS buffer (Sham) were injected into the tibiae of SCID mice. Ten weeks´ post-inoculation, radiography revealed larger osteoblastic lesions (white arrows) in mice injected with PC3c-T1E4 cells compared to those injected with PC3c-CT cells. PC3c-CT-injected mice showed both osteoblastic lesions and osteolytic destructions (white asterisks). Multiple mice of each group were analyzed, and representative radiographies are shown. (**B**) Comparison of bone destruction area (left panel; n=8, P=0.0048) and bone formation area (right panel; n=8, P=0.0032). Two-tailed Mann-Whitney t test. (**C**) 3D micro-CT reconstructions of tibiae implanted with PC3c-CT or PC3c-T1E4 cells and PBS buffer (Sham). Multiple mice of each group were analyzed, and representative radiographies are shown. (**D**) Comparison of bone volume over total tissue volume (BV/TV, %) between tibiae bearing PC3c-CT or PC3c-T1E4 cells (n=8, P=0.0207, two-tailed Mann-Whitney t test). (**E**) Goldner's trichrome staining of bone sections. Multiple mice of each group were analyzed, and representative images are shown. (**F**) Comparison of tumor burden over total soft tissue volume (TB/STV, %) between tibiae bearing PC3c-CT or PC3c-T1E4 cells (n=8, P=NS, two-tailed Mann-Whitney t test). (**G**) TRAP staining of tibiae. Six mice of each group were analyzed, and representative images are shown. (**H**) Comparison of osteoclast surface over bone surface (OC.S/BS, %) between tibiae bearing PC3c-CT or PC3c-T1E4 cells (n=6, P=0.0125, two-tailed unpaired t test). (**I**) Immunohistochemistry detection of Ki67 and ERG in tumors induced by PC3c-CT and PC3c-T1E4 cells. T, Tumor; BM, Bone Matrix; OC, Osteoclasts; GP, Growth Plate.

Fig. 2. The expression of TMPRSS2:ERG in PC3 cells enhances their capacity to reduce osteolysis. (**A**) PC3 cells expressing empty vector (PC3-CT) and T1E4 (PC3-T1E4) were

injected into the tibiae of SCID mice. Four weeks´ post-inoculation, radiography revealed smaller osteolytic lesions (white asterisks) in mice injected with PC3-T1E4 cells compared to those injected with PC3-CT cells. Multiple mice of each group were analyzed, and representative radiographies are shown. (**B**) Comparison of bone destruction area (PC3-CT: n=10, PC3-T1E4: n=11, P=0.0142, two-tailed Mann-Whitney t test). (**C**) 3D micro-CT reconstructions of tibiae implanted respectively with PC3-CT and PC3-T1E4 cells. Multiple mice of each group were analyzed, and representative radiographies are shown. (**D**) Comparison of bone volume over total tissue volume (BV/TV, %) between tibiae bearing PC3-CT or PC3-T1E4 cells (PC3-CT: n=10, PC3-T1E4: n=11, P=0.0400, two-tailed Mann-Whitney t test). (**E**) Goldner's trichrome staining of bone sections from tibiae injected with PC3-CT or PC3-T1E4. Multiple mice of each group were analyzed, and representative radiographies are shown. (**F**) Comparison of tumor burden over total soft tissue volume (TB/STV, %) between tibiae bearing PC3-CT or PC3-T1E4 cells (PC3-CT: n=10, PC3-T1E4: n=11, P=0.0016, two-tailed Mann-Whitney t test). (**G**) TRAP staining of tibiae bearing PC3-CT or PC3-T1E4 cells. Five mice of each group were analyzed, and representative images are shown. (**H**) Comparison of osteoclast surface over bone surface (OC.S/BS, %) between tibiae bearing PC3-CT or PC3-T1E4 cells (n=5, P=0.0496, two-tailed unpaired t test). (**I**) Immunohistochemistry detection of Ki67 and ERG in tumors induced by PC3-CT and PC3-T1E4 cells. T, Tumor; BM, Bone Matrix; OC, Osteoclasts; GP, Growth Plate.

Fig. 3. The expression of the TMPRSS2:ERG fusion enhances osteomimicry properties of PCa cells. (**A** and **C**) Von Kossa staining was performed on control PC3c-CT and PC3c-T1E4 cells (**A**) and on control PC3-CT and PC3-T1E4 cells (**C**) both of which were cultured in osteogenic conditions for 21 days. Von Kossa staining shows mineralization (black zones) and ALPL activity (in pink) (e.g., PC3c-T1E4 cells). (**B** and **D**) Comparison of the expression of the osteogenic markers *ALPL*, *COL1A1*, *OPN*, *BSP*, *OCN*, *OPG* and *RANKL* evaluated by

RT-qPCR between control PC3c-CT and PC3c-T1E4 cells (**B**) and between control PC3-CT and PC3-T1E4 cells (**D**) both cultured in osteogenic conditions for 21 days (P values are indicated on each graph, two-tailed unpaired t test). Bar= 200 μM.

Fig. 4. The upregulation of *ERG* correlates with *ET-1* and the osteogenic markers, *ALPL*, *COL1A1* and *OPN*. cBioPortal platform analysis of a publicly available dataset of human castration resistant prostate adenocarcinoma metastasis samples (n=52, P<0.0001, Fisher's exact test) [25]. Each vertical lane represents one patient, and those shaded in dark-grey highlight the presence of mRNA upregulation.

Fig. 5. ERG directly controls the expression of *ALPL* and *COL1A1* in PCa cells. (**A-L**) The expression of *ERG*, *ALPL* and *COL1A1* were analyzed using RT-qPCR in fusion-positive VCaP cells treated with either control or ERG siRNA (**A**, **B** and **C** respectively) (n=3, ***P<0.001, one-way analysis of variance (ANOVA) with Dunnett's multiple comparison test), in fusion-positive VCaP cells treated with either ethanol vehicle (Veh) or dihydrotestosterone (DHT) to enhance ERG expression (**D**, **E** and **F** respectively) (n=3, P=0.0001, P<0.0001 and P=0.0251 respectively, unpaired t test), in the control PC3c-CT cells and PC3c-T1E4 cells expressing distinct levels (H: high; M: medium; L: low) of T1E4 fusion (**G**, **H** and **I** respectively) (n=3, **P<0.01 and ***P<0.001, one-way analysis of variance (ANOVA) with Dunnett's multiple comparison test), and in PC3c-T1E4-H cells treated with either control or ERG siRNA (**J**, **K** and **L** respectively) (n=3, **P<0.01 and ***P<0.001, one-way analysis of variance (ANOVA) with Dunnett's multiple comparison test). The expression levels of *ERG*, *ALPL* and *COL1A1* found in cells treated with control siRNA were normalized to 1. (**M-N**) ERG binding to the *ALPL* (**M**) and *COL1A1* (**N**) locus were analyzed using ChIP-qPCR in PC3c-T1E4-H and control PC3c-CT cells. The ERG binding sites identified in VCaP cells by ChIP-seq (as shown in **Supplemental Figure 1 and 2**) were

analyzed. Non-specific rabbit-IgG antibody was used as a negative control. (n=3, ***P<0.001, one-way analysis of variance (ANOVA) with Dunnett's multiple comparison test).

Fig. 6. ERG transcription factor regulates *ET-1* gene expression in PCa. (**A**) The expression of *ET-1* was analyzed by RT-qPCR in the control PC3c-CT cells and PC3c-T1E4 cells expressing distinct levels (H: high; M: medium; L: low) of T1E4 fusion (n=3, ***P<0.001, one-way analysis of variance (ANOVA) with Dunnett's multiple comparison test). (**B**) The expression of the ET-1 protein was evaluated based on an ELISA of the conditioned media collected from the parental PC3c cells, control PC3c-CT cells and PC3c-T1E4 cells expressing distinct level (H: high; M: medium; L: low) of T1E4 fusion (n=3, ***P<0.001, one-way analysis of variance (ANOVA) with Dunnett's multiple comparison test). (**C-E**) The expression of *ET-1* was analyzed by RT-qPCR in PC3c-T1E4-H cells treated with either control or ERG siRNA (**C**) (n=3, ***P<0.001, one-way analysis of variance (ANOVA) with Dunnett's multiple comparison test), in fusion-positive VCaP cells treated with either control or ERG siRNA (**D**) (n=3, ***P<0.001, one-way analysis of variance (ANOVA) with Dunnett's multiple comparison test), and in fusion-positive VCaP cells treated with either ethanol vehicle (Veh) or dihydrotestosterone (DHT) to enhance ERG expression (**E**) (n=3, P<0.0001, unpaired t test). The expression levels of *ET-1* found in cells treated with control siRNA were normalized to 1. (**F-H**) The binding of ERG at the *ET-1* locus was analyzed using ChIP-qPCR in PC3c-T1E4-H and control PC3c-CT cells. All three ERG binding sites ((1), (2) and (3)) identified in VCaP cells by ChIP-seq (shown in **Supplemental Figure 3**) were analyzed (**F**), (**G**) and (**H**) respectively. Non-specific rabbit-IgG was used as a negative control (n=3, ***P<0.001, one-way analysis of variance (ANOVA) with Dunnett's multiple comparison test).

Fig. 7. ERG and ET-1 expression are associated in fusion-positive human bone metastasis samples. Immunohistochemistry staining using ERG or ET-1 specific antibodies in *TMPRSS2:ERG*-negative and -positive PCa bone (n=5) and lymph node (n=3) metastasis samples (Histo-pathological characterization of these samples in Supplemental Table 2). Representative images were shown. T: Tumor cells; BV: Blood vessel; BM: Bone matrix; LT: Lymphoid tissue.

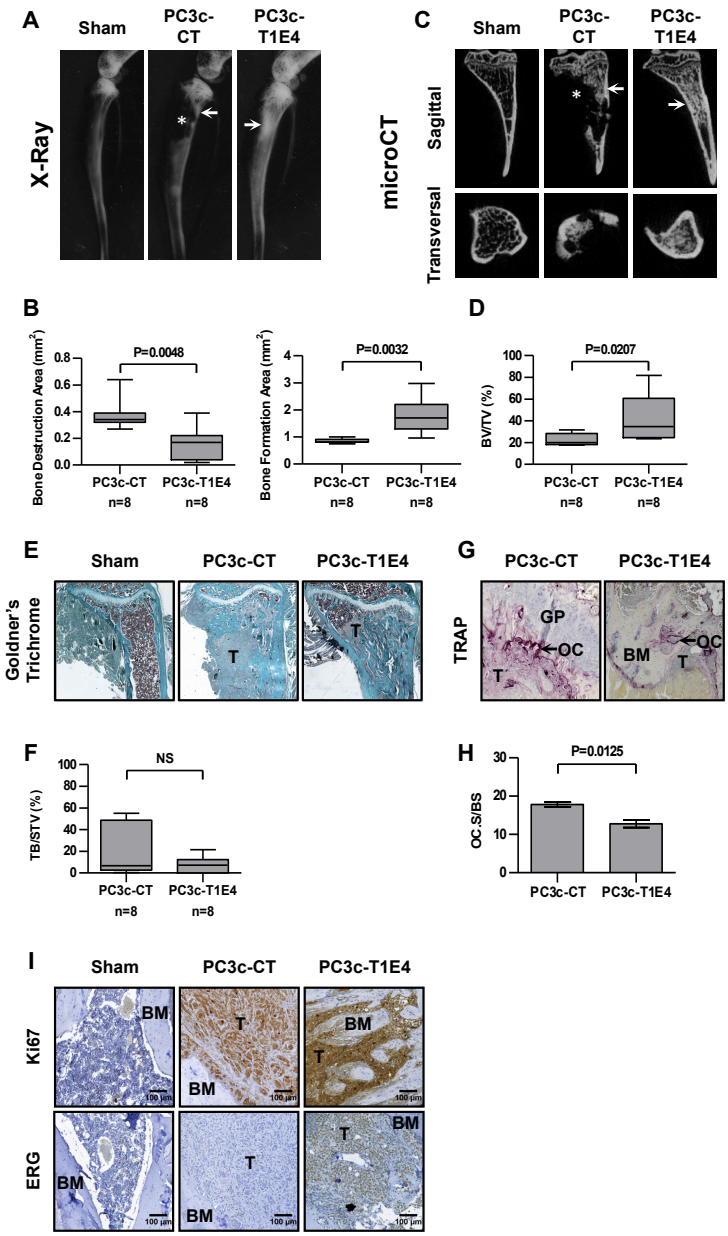

Figure 1
Delliaux et al., 2018

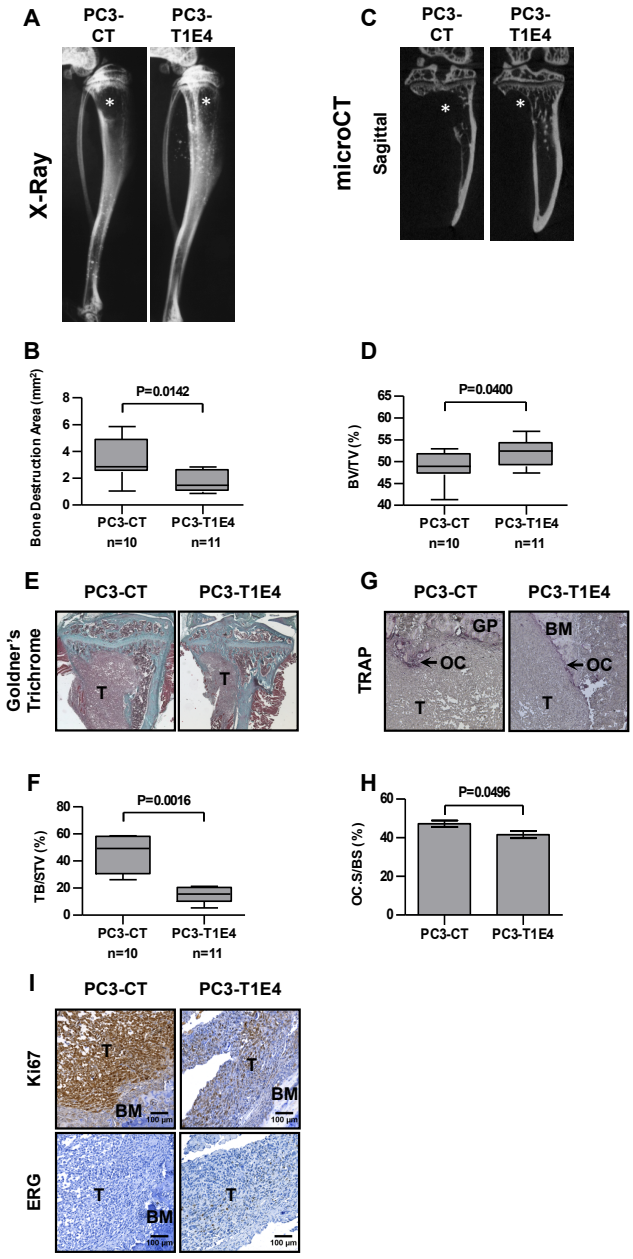

Figure 2
Delliaux et al., 2018

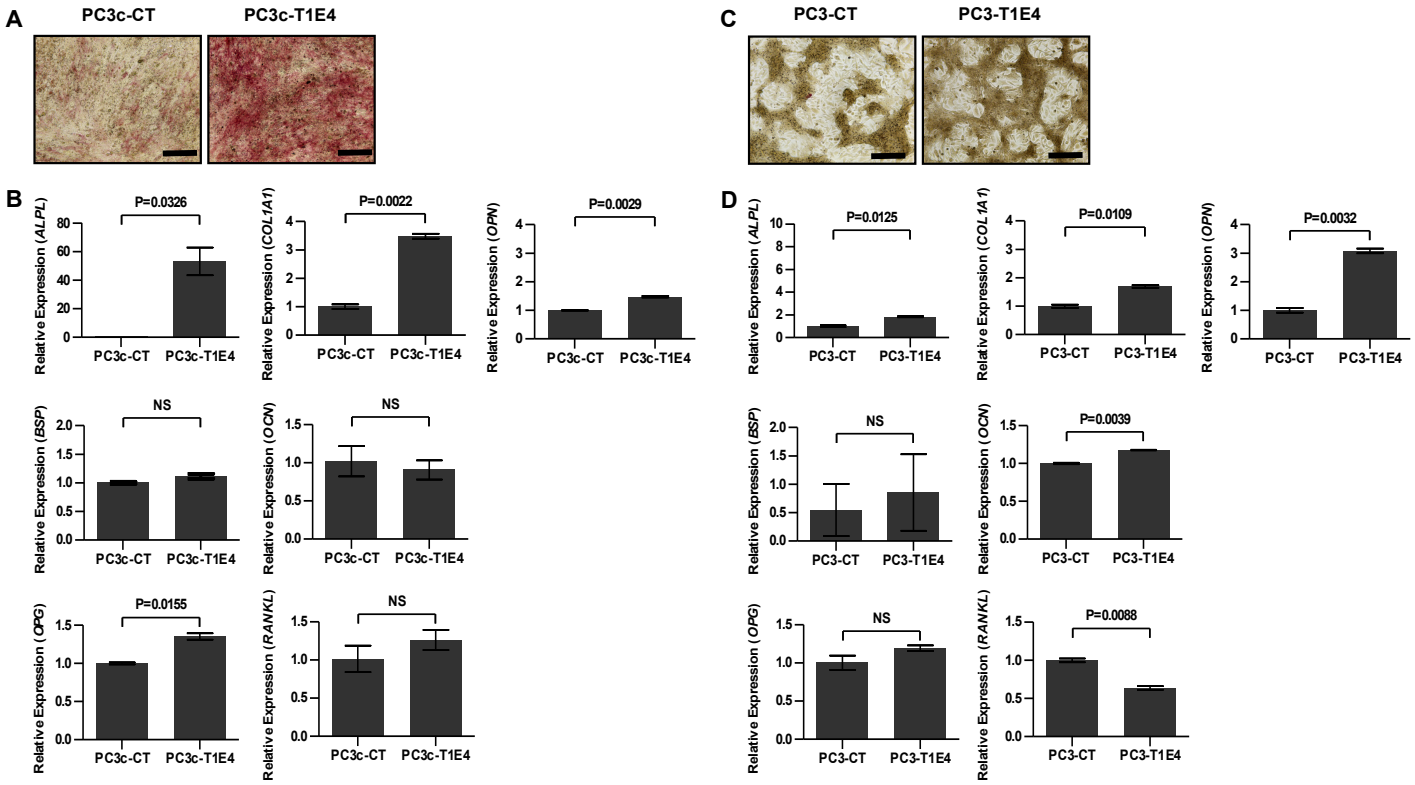

Figure 3
Delliaux et al., 2018

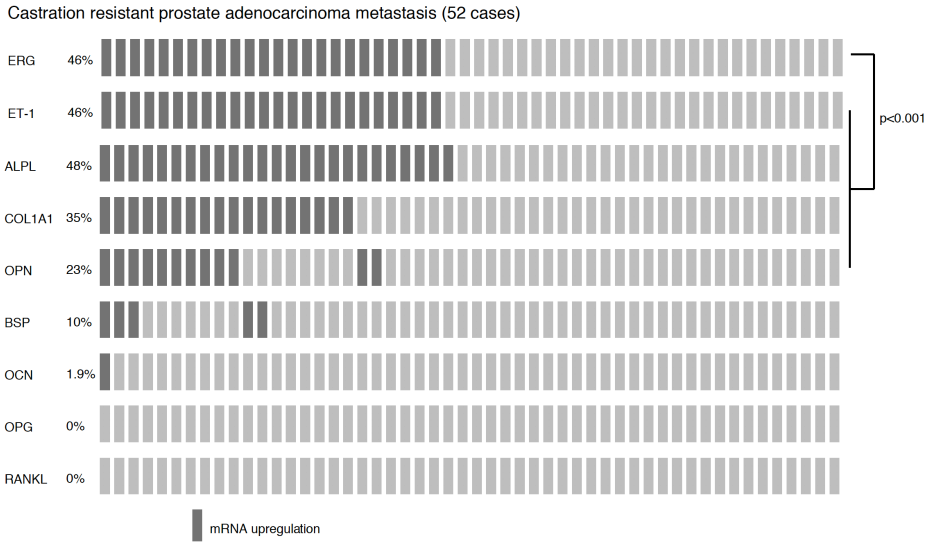

Figure 4
Delliaux et al., 2018

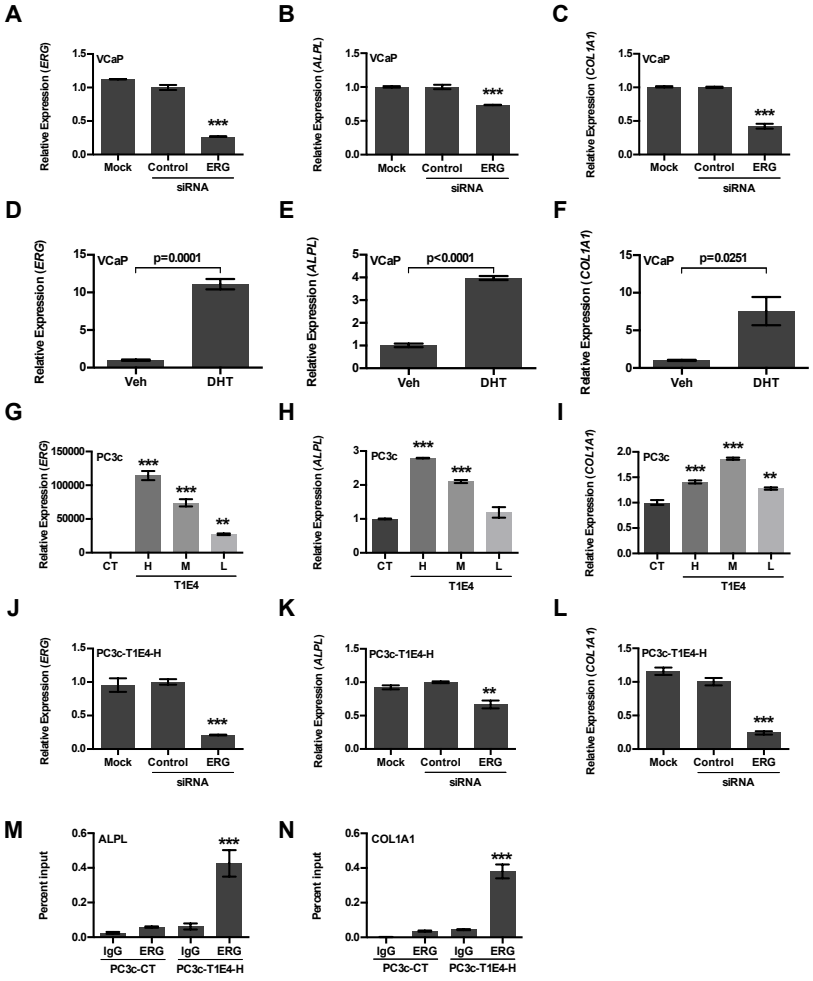

Figure 5
Delliaux et al., 2018

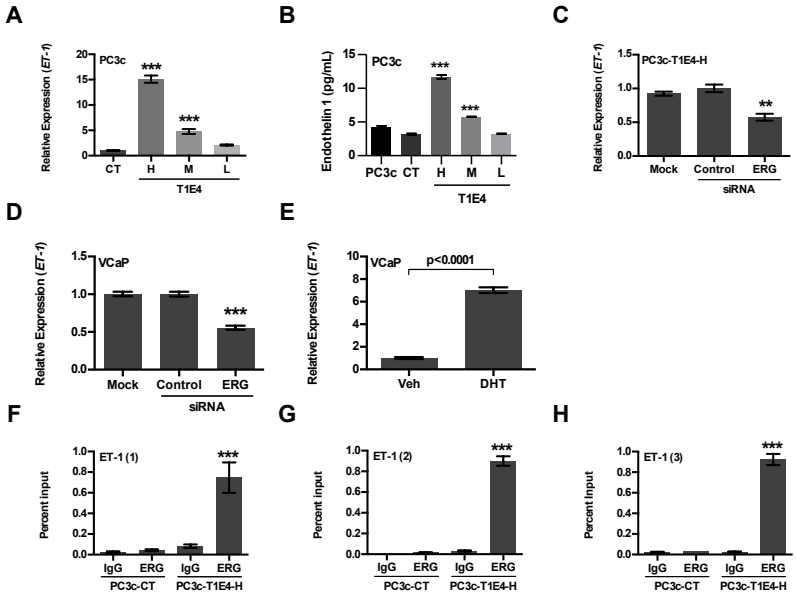

Figure 6
Delliaux et al., 2018

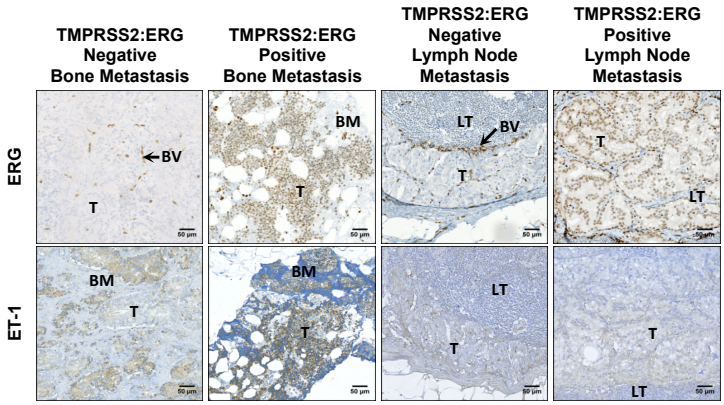

Figure 7
Delliaux et al., 2018

Highlights

- *TMPRSS2:ERG* gene expression enhances the osteoblastic phenotype of bone lesions
- TMPRSS2:ERG fusion-expressing tumor cells overexpress osteoblastic markers
- Expression of *Collagen Type I Alpha 1 Chain, Alkaline Phosphatase* and *Endothelin-1* is enhanced by the TMPRSS2:ERG expression
- *Collagen Type I Alpha 1 Chain*, *Alkaline Phosphatase* and *Endothelin-1* are direct target genes of ERG transcription factor